

SRG operator evolution

A. J. Tropiano¹, S. K. Bogner², R. J. Furnstahl¹

¹*Department of Physics, The Ohio State University, Columbus, OH 43210, USA*

²*National Superconducting Cyclotron Laboratory and Department of Physics and Astronomy,
Michigan State University, East Lansing, MI 48824, USA*

(Dated: August 8, 2019)

Abstract

Brief description of project.

CONTENTS

I. Introduction	3
II. Mathematical/computational details	3
A. Building SRG unitary transformations	3
B. Momentum projection operator: $a_q^\dagger a_q$	3
C. Momentum distribution function: $\phi^2(k)$	4
III. Results	4
A. Entem-Machleidt N ³ LO non-local potential	4
B. RKE N ³ LO and N ⁴ LO semi-local potentials	8
C. Gezerlis N ² LO local potentials	16
References	19

I. INTRODUCTION

Results on SRG-evolved operators from several NN potentials.

- How operators evolve from band- and block-diagonal SRG transformations.
- Operator evolution for different potentials (regulators, chiral order, etc.)

II. MATHEMATICAL/COMPUTATIONAL DETAILS

A. Building SRG unitary transformations

Diagonalize initial and evolved Hamiltonians which we will call $H(0)$ and $H(s)$, respectively. This gives $\psi_\alpha(0)$ and $\psi_\alpha(s)$ for each eigenvalue indexed by α . Then the SRG unitary transformation can be computed by taking a sum over outer products of the evolved and initial wave functions:

$$U(s) = \sum_{\alpha=1}^N |\psi_\alpha(s)\rangle \langle \psi_\alpha(0)|, \quad (1)$$

where N is the dimension of the Hamiltonian matrix. Here the weights are factored into the wave functions, thus $U(s)$ is unitless.

To evolve operators, we simply apply $U(s)$:

$$O(s) = U(s)O(0)U^\dagger(s), \quad (2)$$

where $O(0)$ is the bare operator.

B. Momentum projection operator: $a_q^\dagger a_q$

Applying $a_q^\dagger a_q$ to a wave function $\psi(k)$ returns $\psi(q)$. For the discrete case, $\psi(k_i)$ is an $N \times 1$ vector and $a_q^\dagger a_q(k_i, k_j)$ is an $N \times N$ matrix where $i, j = 1, \dots, N$. Then $a_q^\dagger a_q$ acting on $\psi(k)$ is a matrix multiplication, implying a continuous integration over $d^3k/(2\pi)^3 = 2/(\pi k^2 dk)$ in spherical coordinates. Therefore, we include a factor of $\pi/(2k_i k_j \sqrt{w_i w_j})$ in $a_q^\dagger a_q(k_i, k_j)$ where w represents the momentum weights. In matrix form,

$$a_q^\dagger a_q(k_i, k_j) = \frac{\pi \delta_{k_i q} \delta_{k_j q}}{2k_i k_j \sqrt{w_i w_j}}, \quad (3)$$

which has units fm^3 . To evolve operators, we apply $U(s)$ at this point. For mesh-independent figures, we must divide by an additional factor of $k_i k_j \sqrt{w_i w_j}$.

C. Momentum distribution function: $\phi^2(k)$

We diagonalize the Hamiltonian for eigenvectors ψ_α . In the 3S_1 - 3D_1 coupled channel, the S-component is given by $\psi_\alpha[:N]$ and the D-component by $\psi_\alpha[N:]$ where N is the length of the momentum mesh. Then the momentum distribution of the state α is given by,

$$|\phi_\alpha(k)|^2 = |\psi_\alpha[:N]|^2 + |\psi_\alpha[N:]|^2. \quad (4)$$

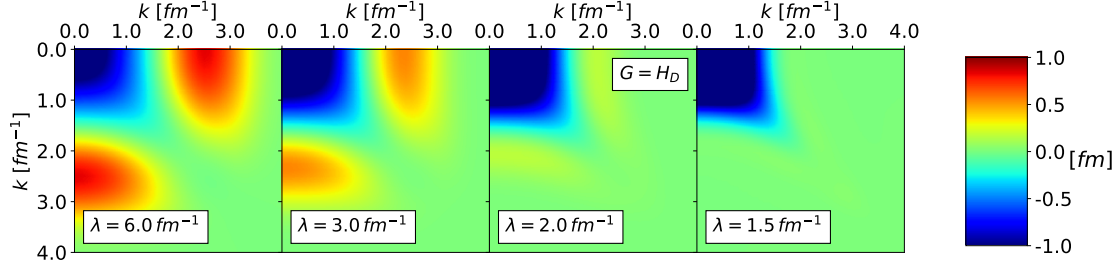
This satisfies the normalization condition $\sum_{i=1}^N |\phi(k_i)|^2 = 1$, implying that the factor $k^2 dk$ (or in the discrete case, $k_i^2 w_i$) is factored into the wave function. For mesh-independent figures, divide by $k_i^2 w_i$.

III. RESULTS

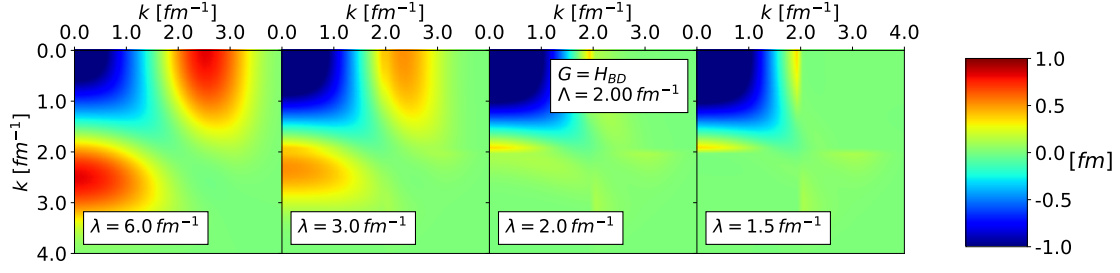
Organize this according to the figures. Format should be description of the calculation (previous section), followed by the figure, followed by takeaways.

A. Entem-Machleidt $N^3\text{LO}$ non-local potential

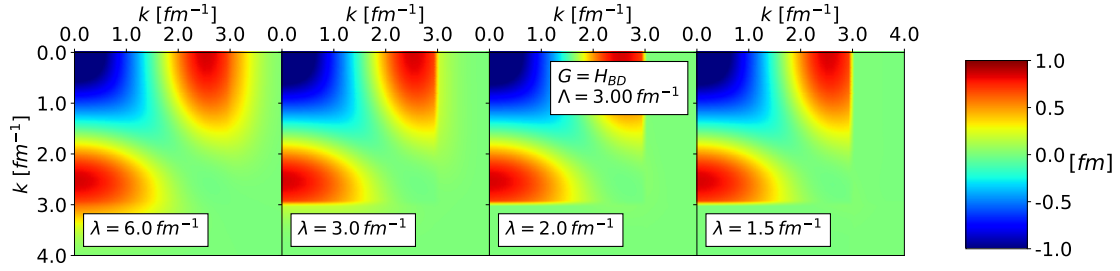
Non-local potential from [1].



(a)



(b)



(c)

FIG. 1: Matrix elements of the Entem-Machleidt N³LO non-local potential $V_\lambda(k, k')$ SRG-evolving in λ right to left under transformations with the Wegner generator (a) and block-diagonal generators decoupling at $\Lambda = 2$ and 3 fm^{-1} (b and c).

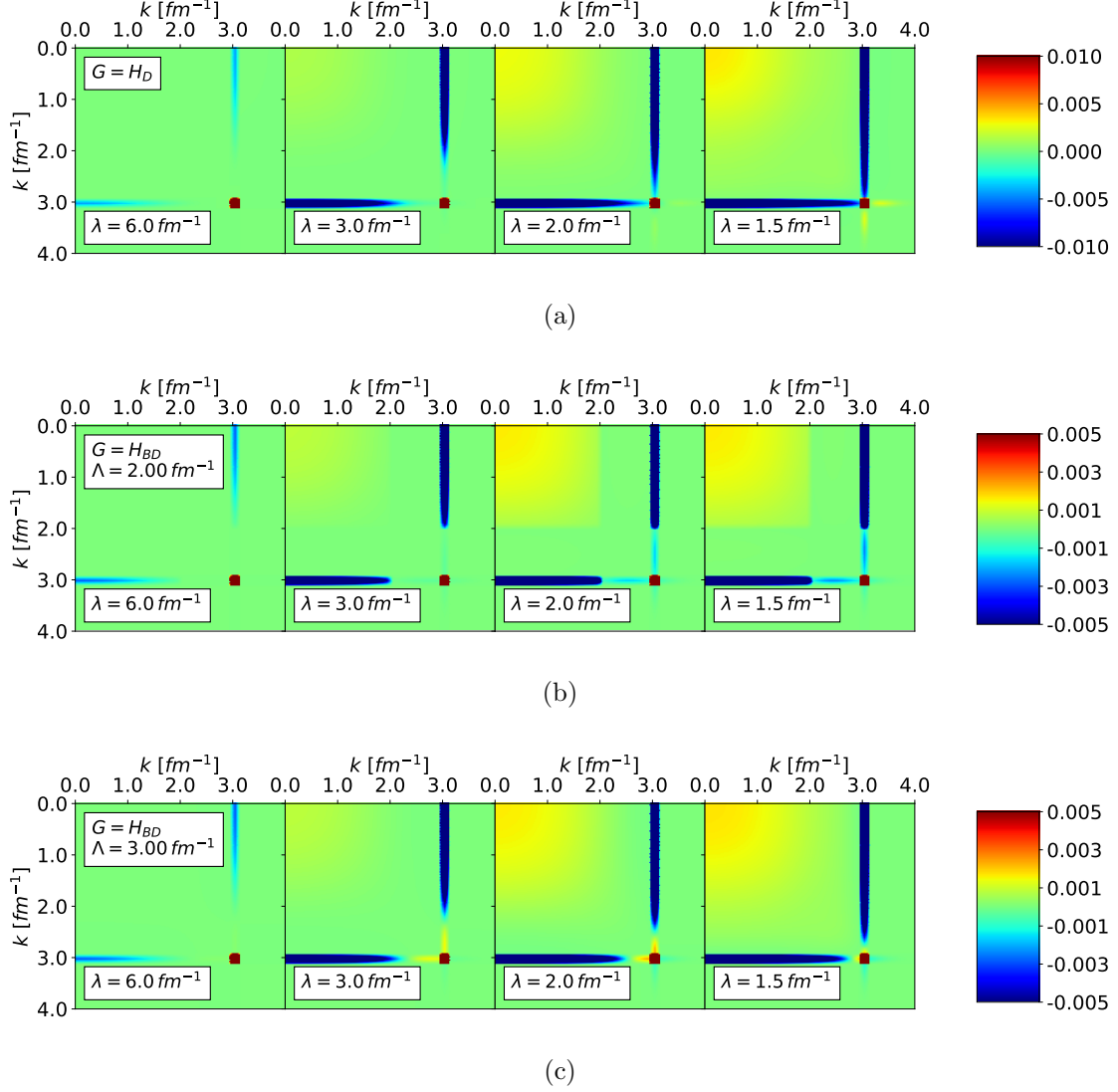


FIG. 2: Matrix elements of $\langle k|a_q^\dagger a_q|k'\rangle$ SRG-evolving in λ right to left under transformations from the Entem-Machleidt N³LO non-local potential with the Wegner generator (a) and block-diagonal generators decoupling at $\Lambda = 2$ and 3 fm^{-1} (b and c). Here $q = 3 \text{ fm}^{-1}$.

- The top row of Fig. 2 should match the top row in Fig. 4 of [2].
- Smeared delta function comment.
- Compared block-diagonal to Wegner.
- Another note about block-diagonal.

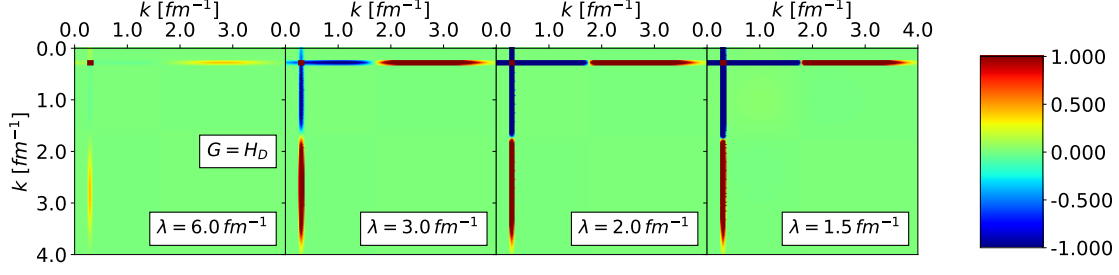


FIG. 3: Matrix elements of $\langle k | a_q^\dagger a_q | k' \rangle$ SRG-evolving in λ right to left under transformations from the Entem-Machleidt N³LO non-local potential with the Wegner generator. Here $q = 0.3 \text{ fm}^{-1}$.

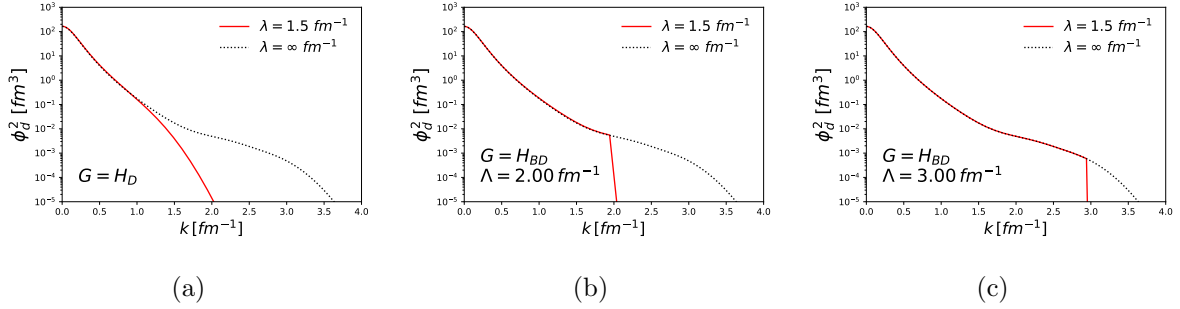


FIG. 4: Momentum probability densities of the deuteron SRG-evolving the wave function to $\lambda = 1.5 \text{ fm}^{-1}$ from the Entem-Machleidt N³LO non-local potential with the Wegner generator (a) and block-diagonal generators decoupling at $\Lambda = 2$ and 3 fm^{-1} (b and c). The black dotted line corresponds to the momentum probability density of the initial deuteron wave function.

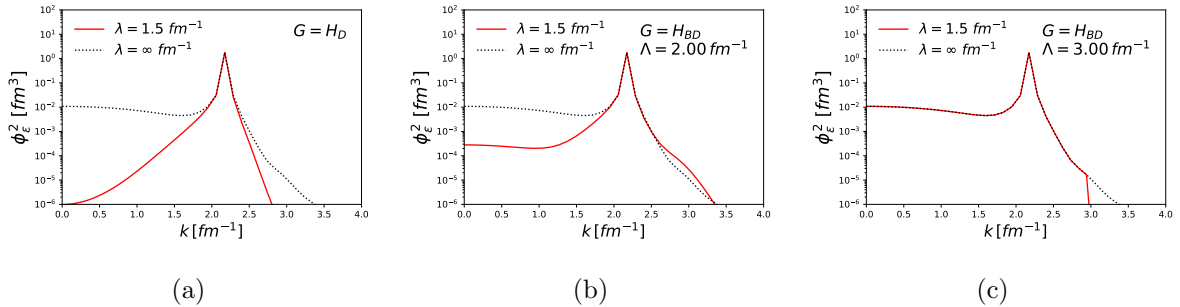


FIG. 5: Momentum probability densities of the continuum state at $\epsilon \approx 200 \text{ MeV}$ SRG-evolving the wave function to $\lambda = 1.5 \text{ fm}^{-1}$ from the Entem-Machleidt N³LO non-local potential with the Wegner generator (a) and block-diagonal generators decoupling at $\Lambda = 2$ and 3 fm^{-1} (b and c). The black dotted line corresponds to the initial momentum probability density.

B. RKE N³LO and N⁴LO semi-local potentials

Add takeaways for these figures. Semi-local potentials from [3].

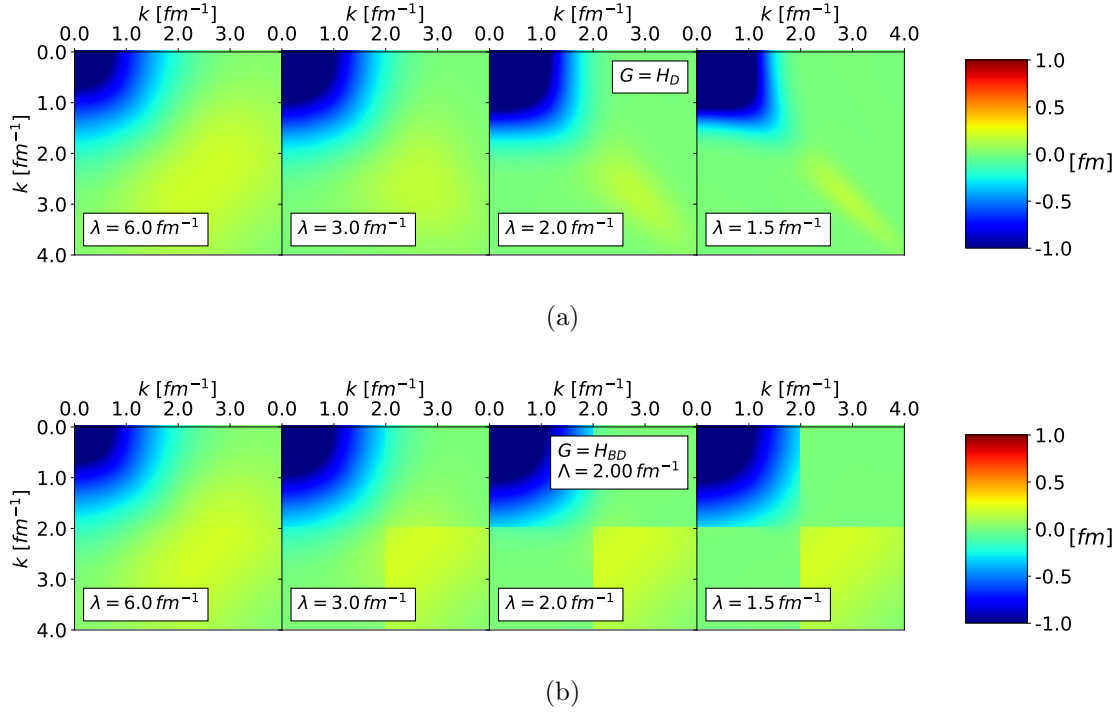
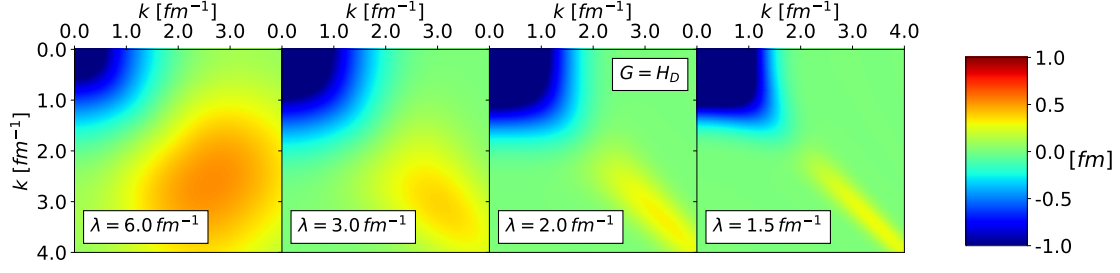
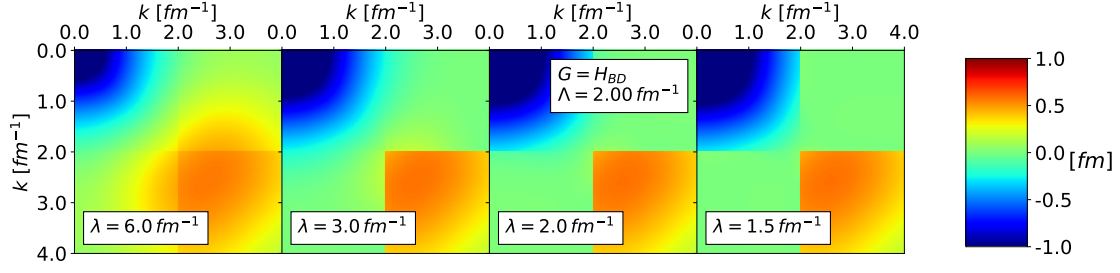


FIG. 6: Matrix elements of the RKE N³LO semi-local potential $V_\lambda(k, k')$ SRG-evolving in λ right to left under transformations with the Wegner generator (a) and block-diagonal generator decoupling at $\Lambda = 2 \text{ fm}^{-1}$ (b). Here the EFT cutoff is 450 MeV.

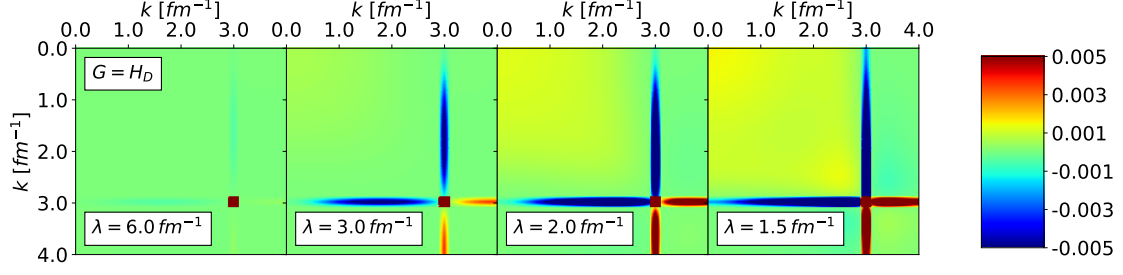


(a)

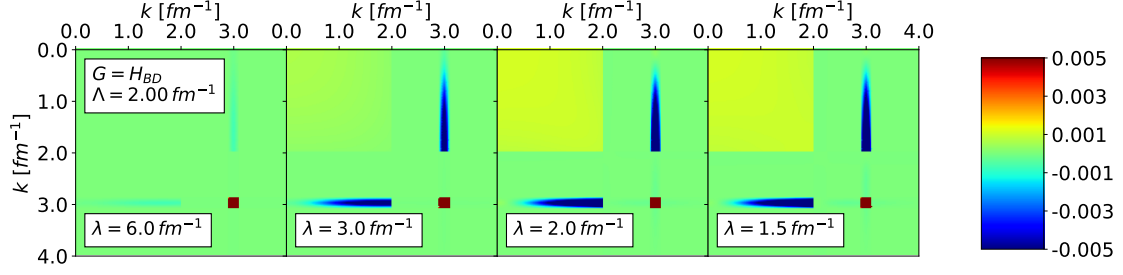


(b)

FIG. 7: Matrix elements of the RKE N³LO semi-local potential $V_\lambda(k, k')$ SRG-evolving in λ right to left under transformations with the Wegner generator (a) and block-diagonal generator decoupling at $\Lambda = 2 \text{ fm}^{-1}$ (b). Here the EFT cutoff is 500 MeV.

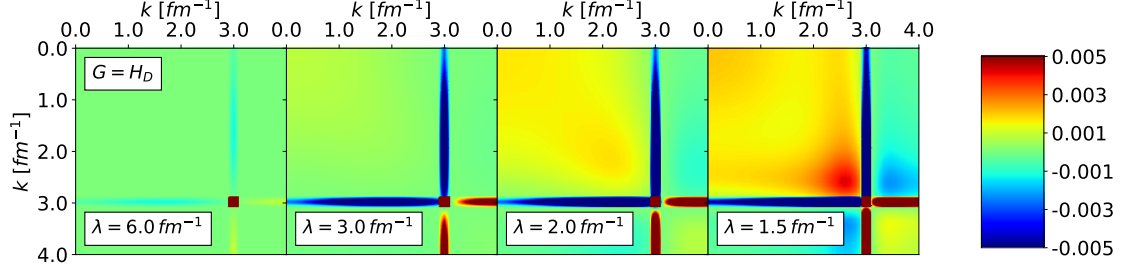


(a)

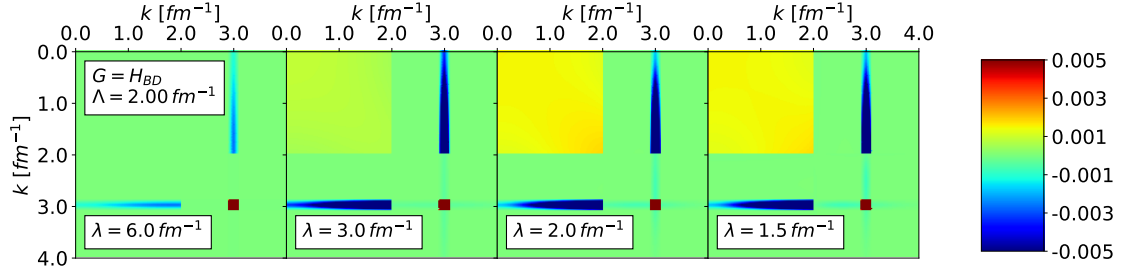


(b)

FIG. 8: Matrix elements of $\langle k|a_q^\dagger a_q|k'\rangle$ SRG-evolving in λ right to left under transformations from the RKE N³LO semi-local potential with the Wegner generator (a) and block-diagonal generator decoupling at $\Lambda = 2 \text{ fm}^{-1}$ (b). Here $q = 3 \text{ fm}^{-1}$ and the EFT cutoff is 450 MeV.

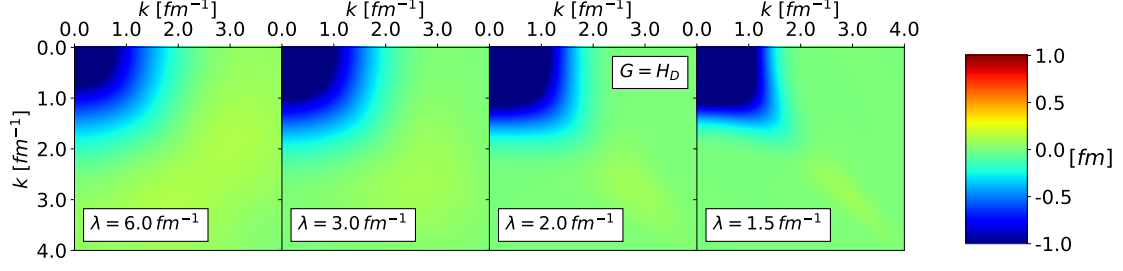


(a)

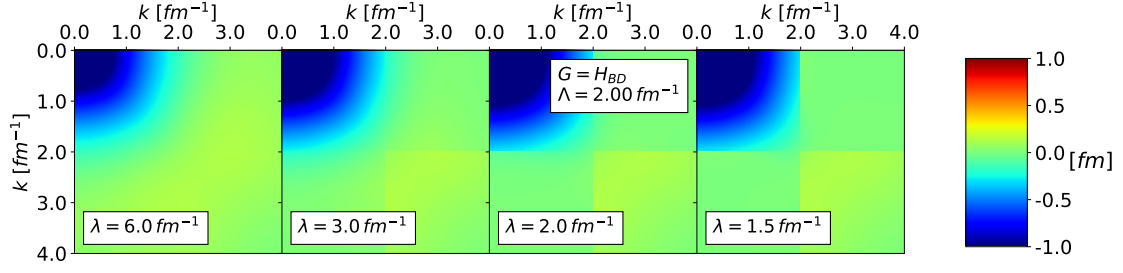


(b)

FIG. 9: Matrix elements of $\langle k|a_q^\dagger a_q|k'\rangle$ SRG-evolving in λ right to left under transformations from the RKE N³LO semi-local potential with the Wegner generator (a) and block-diagonal generator decoupling at $\Lambda = 2 \text{ fm}^{-1}$ (b). Here $q = 3 \text{ fm}^{-1}$ and the EFT cutoff is 500 MeV.

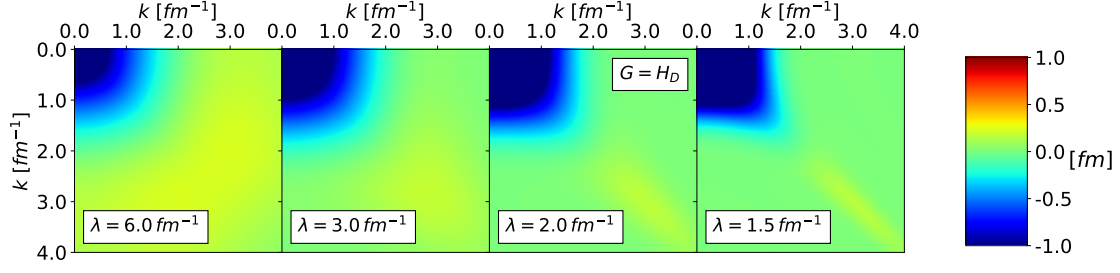


(a)

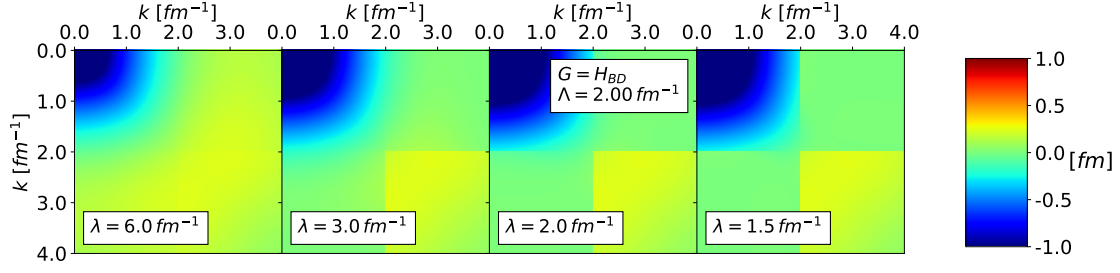


(b)

FIG. 10: Matrix elements of the RKE N⁴LO semi-local potential $V_\lambda(k, k')$ SRG-evolving in λ right to left under transformations with the Wegner generator (a) and block-diagonal generator decoupling at $\Lambda = 2 \text{ fm}^{-1}$ (b). Here the EFT cutoff is 450 MeV.

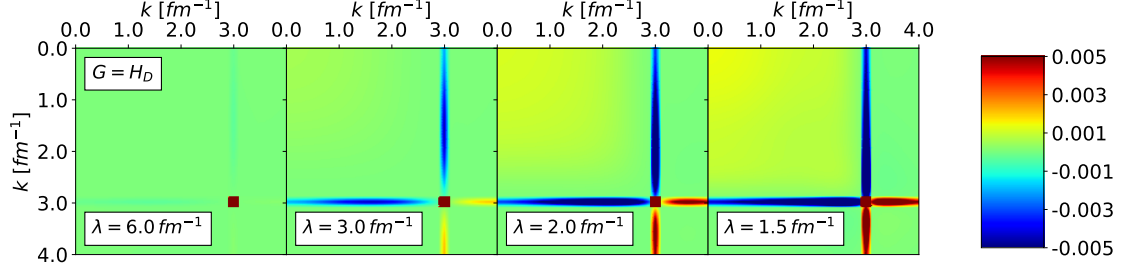


(a)

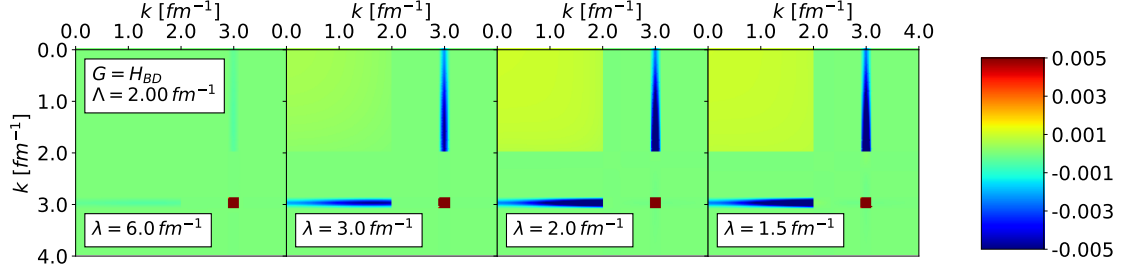


(b)

FIG. 11: Matrix elements of the RKE $N^4\text{LO}$ semi-local potential $V_\lambda(k, k')$ SRG-evolving in λ right to left under transformations with the Wegner generator (a) and block-diagonal generator decoupling at $\Lambda = 2 \text{ fm}^{-1}$ (b). Here the EFT cutoff is 500 MeV.



(a)



(b)

FIG. 12: Matrix elements of $\langle k|a_q^\dagger a_q|k'\rangle$ SRG-evolving in λ right to left under transformations from the RKE N⁴LO semi-local potential with the Wegner generator (a) and block-diagonal generator decoupling at $\Lambda = 2 \text{ fm}^{-1}$ (b). Here $q = 3 \text{ fm}^{-1}$ and the EFT cutoff is 450 MeV.

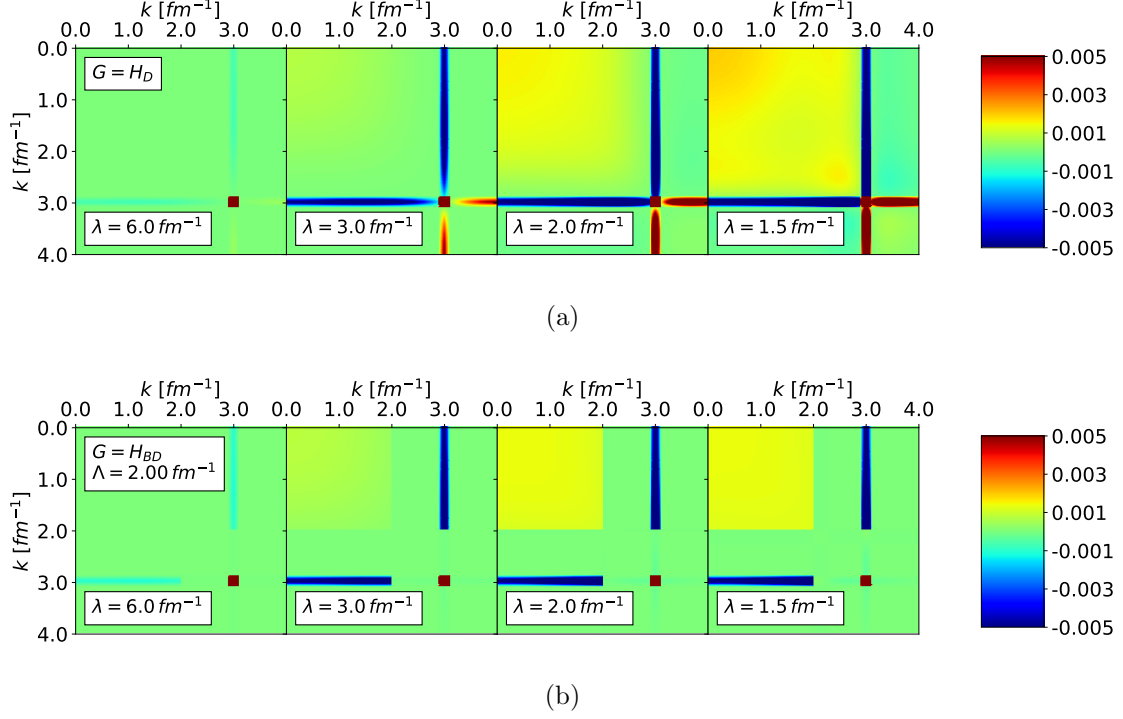


FIG. 13: Matrix elements of $\langle k|a_q^\dagger a_q|k'\rangle$ SRG-evolving in λ right to left under transformations from the RKE N⁴LO semi-local potential with the Wegner generator (a) and block-diagonal generator decoupling at $\Lambda = 2 \text{ fm}^{-1}$ (b). Here $q = 3 \text{ fm}^{-1}$ and the EFT cutoff is 500 MeV.

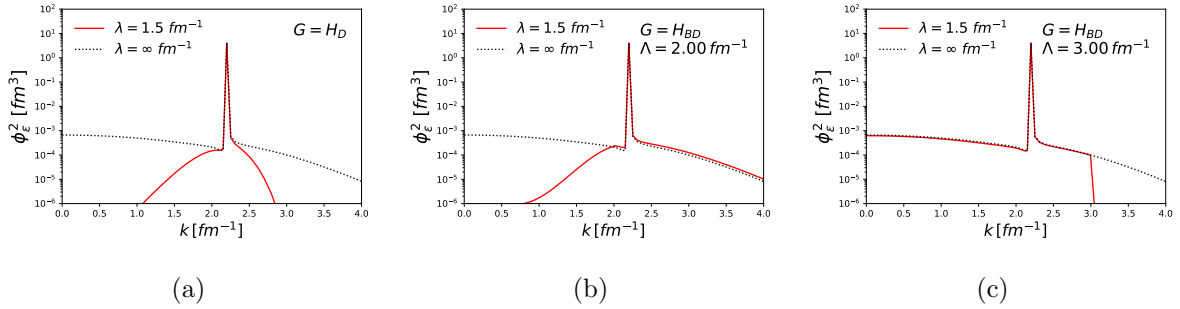


FIG. 14: Momentum probability densities of the continuum state at $\epsilon \approx 200 \text{ MeV}$ SRG-evolving the wave function to $\lambda = 1.5 \text{ fm}^{-1}$ from the RKE N⁴LO semi-local potential with the Wegner generator (a) and block-diagonal generators decoupling at $\Lambda = 2$ and 3 fm^{-1} (b and c). The black dotted line corresponds to the initial momentum probability density. Here the EFT cutoff is 450 MeV.

C. Gezerlis N²LO local potentials

Add takeaways for these figures. Local potentials from [4].

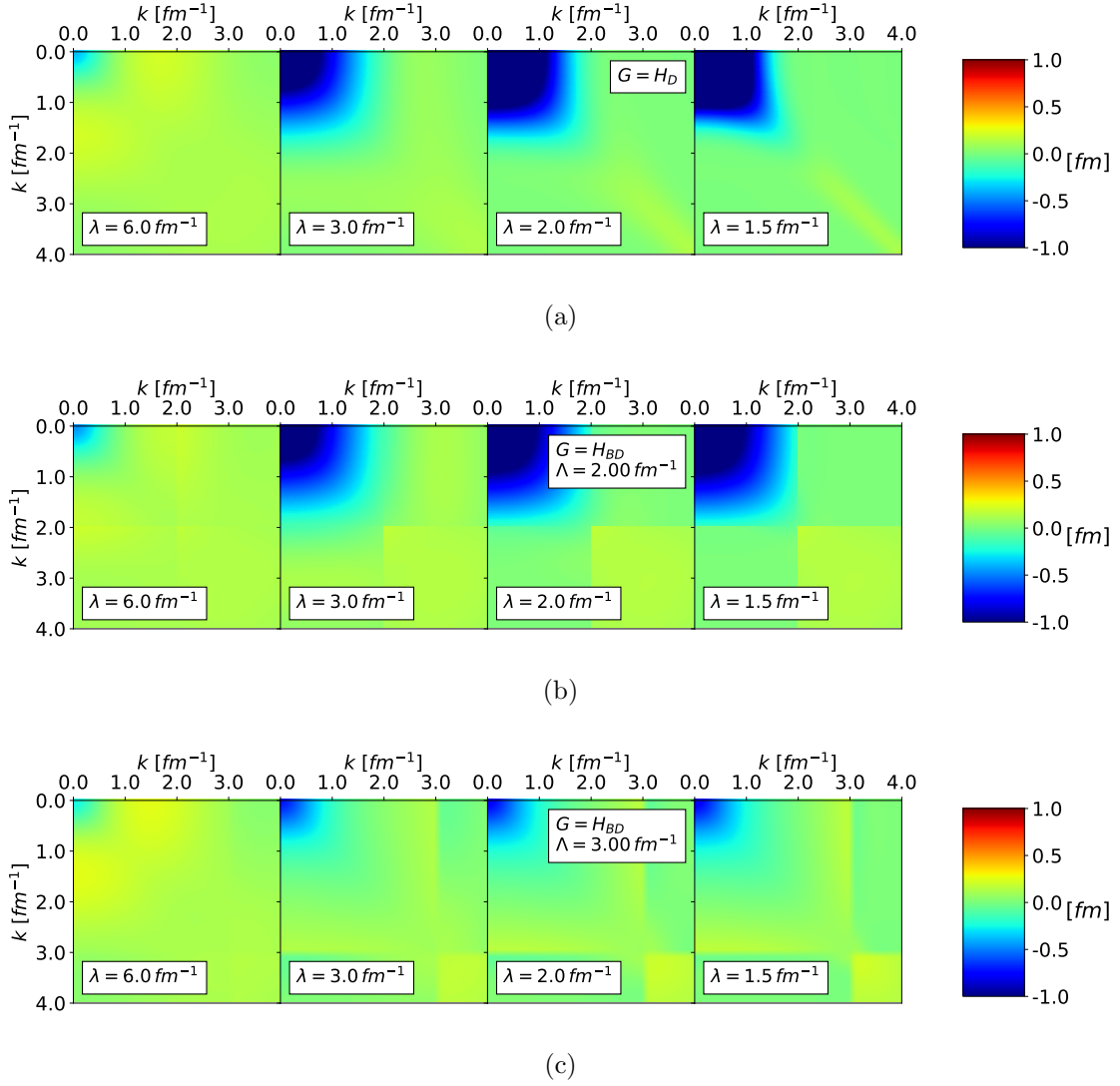
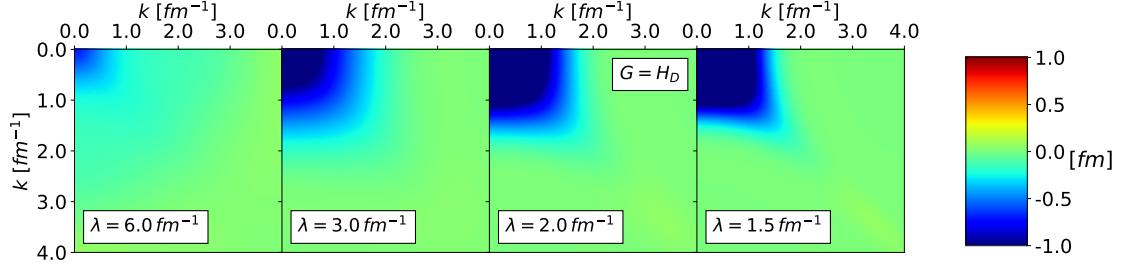
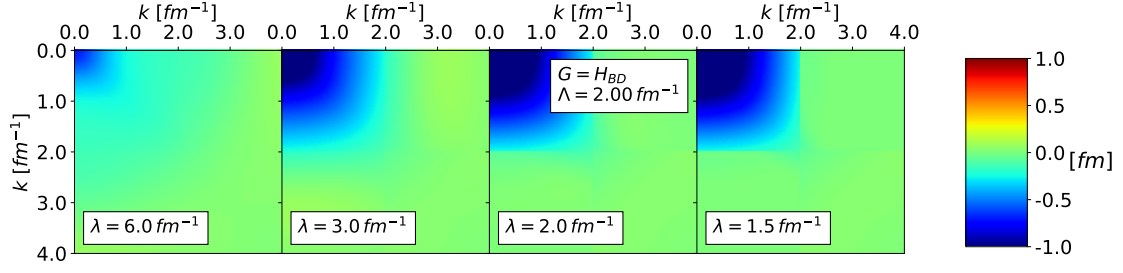


FIG. 15: Matrix elements of the Gezerlis et al. N²LO local potential $V_\lambda(k, k')$ SRG-evolving in λ right to left under transformations with the Wegner generator (a) and block-diagonal generators decoupling at $\Lambda = 2$ and 3 fm^{-1} (b and c). Here the EFT cutoff is 1 fm .

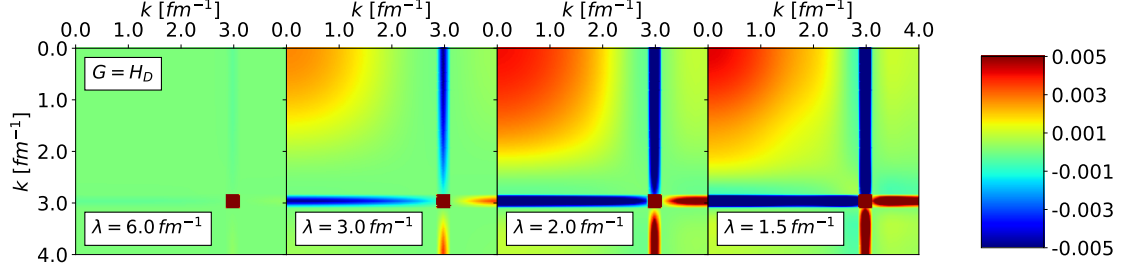


(a)

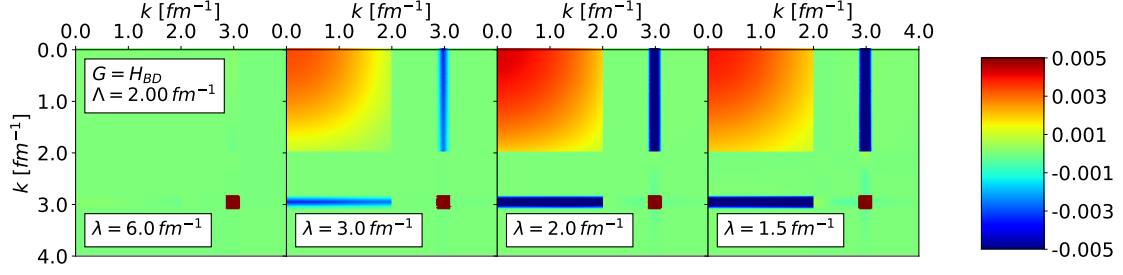


(b)

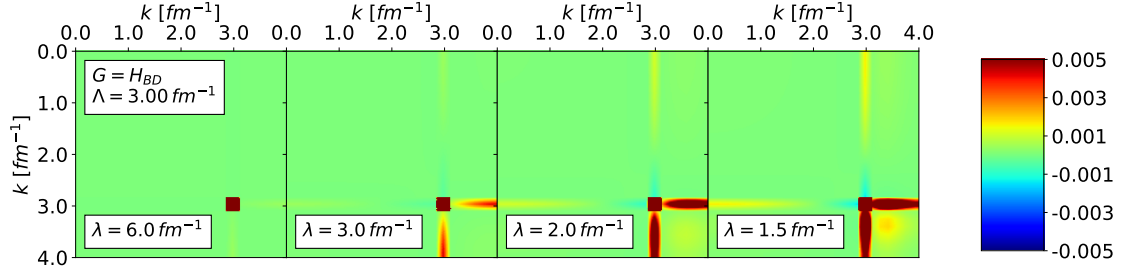
FIG. 16: Matrix elements of the Gezerlis et al. $N^2\text{LO}$ local potential $V_\lambda(k, k')$ SRG-evolving in λ right to left under transformations with the Wegner generator (a) and block-diagonal generator decoupling at $\Lambda = 2 \text{ fm}^{-1}$ (b). Here the EFT cutoff is 1.2 fm.



(a)



(b)



(c)

FIG. 17: Matrix elements of $\langle k|a_q^\dagger a_q|k'\rangle$ SRG-evolving in λ right to left under transformations from the Gezerlis et al. N²LO local potential with the Wegner generator (a) and block-diagonal generators decoupling at $\Lambda = 2$ and 3 fm^{-1} (b and c). Here $q = 3 \text{ fm}^{-1}$ and the EFT cutoff is 1 fm .

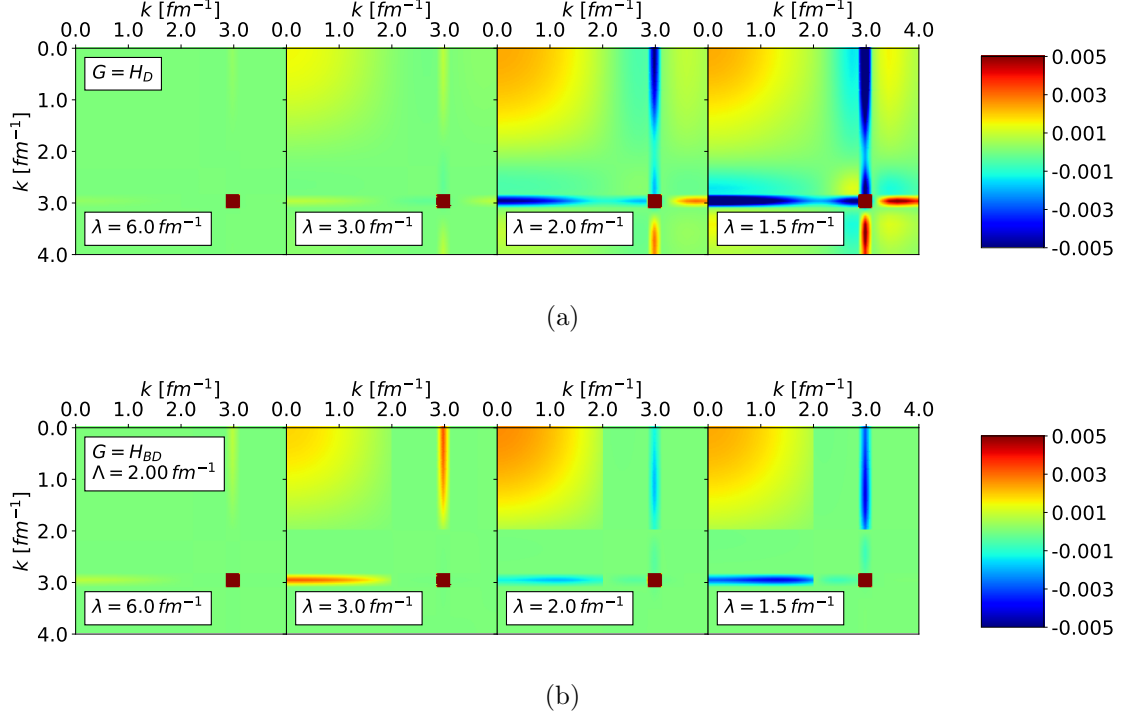


FIG. 18: Matrix elements of $\langle k|a_q^\dagger a_q|k' \rangle$ SRG-evolving in λ right to left under transformations from the Gezerlis et al. $N^2\text{LO}$ local potential with the Wegner generator (a) and block-diagonal generator decoupling at $\Lambda = 2 \text{ fm}^{-1}$ (b). Here $q = 3 \text{ fm}^{-1}$ and the EFT cutoff is 1.2 fm .

-
- [1] D. R. Entem and R. Machleidt, Phys. Rev. C **68**, 041001 (2003), arXiv:nucl-th/0304018 [nucl-th].
 - [2] E. R. Anderson, S. K. Bogner, R. J. Furnstahl, and R. J. Perry, Phys. Rev. C **82**, 054001 (2010), arXiv:1008.1569 [nucl-th].
 - [3] P. Reinert, H. Krebs, and E. Epelbaum, Eur. Phys. J. A **54**, 86 (2018), arXiv:1711.08821 [nucl-th].
 - [4] A. Gezerlis, I. Tews, E. Epelbaum, M. Freunek, S. Gandolfi, K. Hebeler, A. Nogga, and A. Schwenk, Phys. Rev. C **90**, 054323 (2014), arXiv:1406.0454 [nucl-th].